



Confined crystallization in the binary blends of diblock copolymers bearing stereoisomeric isotactic and syndiotactic polypropylene

Che-Yi Chu¹  | Meng-Zhe Chen² | Wun-Hong Li¹ | Jing-Cherng Tsai³ | Hsin-Lung Chen² 

¹Department of Chemical Engineering, National Chung Hsing University, Taichung, Taiwan

²Department of Chemical Engineering, National Tsing Hua University, Hsinchu, Taiwan

³Department of Chemical Engineering, National Chung Cheng University, Chiayi, Taiwan

Correspondence

Che-Yi Chu, Department of Chemical Engineering, National Chung Hsing University, Taichung 402, Taiwan.
Email: cychu0123@dragon.nchu.edu.tw

Hsin-Lung Chen, Department of Chemical Engineering, National Tsing Hua University, Hsinchu 30013, Taiwan.
Email: hslchen@mx.nthu.edu.tw

Funding information

MOST, Grant/Award Number: 108-2221-E-007-021

Abstract

The morphology and crystallization behavior of the binary blends of two crystalline-amorphous diblock copolymers bearing stereoisomeric crystalline blocks have been investigated. A polystyrene-*block*-isotactic polypropylene (S-iPP) and a polystyrene-*block*-syndiotactic polypropylene (S-sPP) were used to prepare a series of blends forming lamellar morphology. In the melt state, the PS blocks from these two diblock copolymers mixed intimately in the PS lamellar microdomains; meanwhile, the iPP and sPP blocks were found to form a miscible mixture in the PP domains. Under the effects of nanoscale confinement and the constraint imposed by the junction points, the iPP and sPP blocks exhibited the crystallization behavior greatly deviated from that in the neat diblock copolymers. A local demixing between a fraction of iPP and sPP chains was found to occur in the S-sPP-rich blend at low crystallization temperatures, which yielded the defective crystalline domains composed of alternately intervened iPP and sPP crystallites. This crystalline species displayed a significant depression of melting point located at the temperature around 10°C higher than the corresponding T_c due to an excess surface free energy at the interface between the alternately intervened iPP and sPP crystallites.

KEYWORDS

block copolymer, confined crystallization, isotactic polypropylene, lamellar microdomain, syndiotactic polypropylene

1 | INTRODUCTION

Nanoconfined crystallization of polymer brushes within the microdomains templated by crystalline-amorphous (C-A) diblock copolymer has received significant attention over the past two decades. In particular, the self-assembly of C-A diblock copolymer into lamellar, cylindrical, and spherical microdomains constituting the crystalline block could impose 1-D, 2-D, and 3-D confinement to the crystallization process, respectively.^{1–3} Under the influence of nanoconfinement, controllable crystallization kinetics,^{4–7} and preferred crystal orientations^{1,6,8–10} have been attained by using various C-A block copolymers as the templates.

The manner of chain confinement exerted by this type of diblock copolymer can be extended to a more complex system, namely, the blends of two C-A diblock copolymers bearing chemically identical A block. In this case, the two C blocks from their respective copolymers could form the common microdomains through the co-surfactant effect.^{11,12} This type of diblock copolymer blend can be classified into the following sub-classes: (1) C_n-b-A_m/C_l-b-A_k blend (with the subscripts denoting the different block lengths), where the two diblocks are chemically identical, and (2) $C_n-b-A_m/C_l'-b-A_k$ blend, where the two crystalline blocks are chemically different. These blend systems would offer an opportunity to examine if the two crystalline blocks

could form an intimate mixture in both melt and crystalline states within the microdomain space driven by the confinement effect as well as the localization of the junction points at the microdomain interface.

Our previous study on the first system formed by the blends of two polybutadiene-*block*-poly(ethylene oxide)s (PB-*b*-PEO) has shown that the PEO blocks of different chain lengths in the blends could co-crystallize over a broad range of undercooling even when the crystallization temperature (T_c) situated well above the glass transition temperature (T_g) of PB block, primarily due to a thermodynamic requirement for attaining a lower interfacial energy and a higher conformational entropy of the longer PB blocks in the system.¹³ We have also investigated crystallization behavior in the second type of system and identified the defective crystalline domains exhibiting a significant depression of the melting point along with a peculiar diffraction peak in the wide angle X-ray scattering (WAXS) profiles in the blends of a polystyrene-*block*-poly(ethylene oxide) (PS-*b*-PEO) and a polystyrene-*block*-poly(L-lactide) (PS-*b*-PLLA).¹⁴ We proposed that the formation of the defective crystalline domains arose from a local demixing between a fraction of PEO and PLLA chains under the influences of restricted chain mobility of PLLA and the junction point constraint, thus generating the tiny PLLA crystallites intervened by the PEO block chains. As the blends of PEO and PLLA homopolymers with relatively low molecular weight were miscible in the melt,^{15–19} the formation of composite microdomains by the PEO and PLLA blocks from their respective copolymers was expected, as that observed in the studies on PS-*b*-PEO/polystyrene-*block*-poly(D,L-lactide) binary blends reported by Mao and Hillmyer^{20–22} and in our previous study.¹⁴ A recent study by Chen et al. further focused on the binary copolymer blends comprising PS-*b*-PEO and polystyrene-*block*-poly(acrylic acid) (PS-*b*-PAA), in which the hydrogen bonding between PEO and PAA blocks improved their miscibility to form the common microdomains and microphase-separated against the domains composed of PS blocks; however, the crystallizable chain length of PEO was reduced by the hydrogen bonds, causing the crystallization to occur within a more confined region.²³

An interesting extension of the second system is the consideration of using two chemically different and immiscible C_n and C_l blocks in their homopolymer state to examine if their miscibility could be improved once the amorphous A_m and A_k blocks could mix intimately with each other. Thus, the present work investigates the miscibility and crystallization behavior of the blends of a polystyrene-*block*-isotactic polypropylene (PS-*b*-iPP) and a polystyrene-*block*-syndiotactic polypropylene (PS-*b*-sPP), where the stereoisomeric iPP and sPP have been considered to be immiscible in their homopolymer blends in the melt state.^{24–26} The origin of their immiscibility was associated with a positive energy change upon forming the blend, as predicted by the Monte Carlo simulation.²⁷ It would hence be of great interest here to investigate the melt miscibility between iPP and sPP blocks within the microdomains formed in the PS-*b*-iPP/PS-*b*-sPP blends. Moreover, it is known that there is a variety of crystal modifications of iPP and sPP, such as α , β , γ , and mesomorphic forms found in iPP^{28–32} and I, II, III, IV and mesomorphic forms observed for sPP^{33–38};

consequently, it will be of our further interest to explore how the spatial confinement affects the interplay between the crystallization of iPP and sPP blocks if they could mix intimately in the microdomain.

In this study, we blend a shorter symmetric PS-*b*-iPP (abbreviated as S-iPP) with a longer asymmetric PS-*b*-sPP (abbreviated as S-sPP) to prepare a series of lamellae-forming blends with different compositions. It will be shown that the binary blends composed of the PS lamellar microdomains formed by the mixture of the PS blocks from the two copolymers and the PP lamellae in which iPP and sPP blocks could mix intimately in the melt state. The crystallization of iPP and sPP blocks over a broad range of T_c confined within the PP microdomains exhibited a significant deviation from that in the neat diblock copolymers, where the crystallization of S-sPP-rich blend at low T_c resulted in the formation of the defective crystalline domains in which the iPP and sPP crystallites intervened each other. This S-sPP-rich blend will also be used to reveal the preferred orientation of iPP and sPP crystallites in their common lamellar microdomains.

2 | EXPERIMENTAL SECTION

2.1 | Materials and sample preparation

PS-*b*-iPP ($M_{n,PS} = 3500$, $M_{n,iPP} = 3800$) and PS-*b*-sPP ($M_{n,PS} = 9400$, $M_{n,sPP} = 6800$) were synthesized according to the procedure reported in the previous studies.^{39,40} The volume fraction of iPP and sPP blocks in the two diblock copolymers in the melt state were 0.54 and 0.46, respectively.

For the blend preparation, the two diblock copolymers with desired weight ratios were dissolved in xylene at 50°C to yield 3 wt% solutions, and followed by casting the solutions on the Petri dishes. The blend films were obtained after evaporating most of the solvent quickly on the hot plate at ca. 140°C (\cong boiling point of xylene). The blend films were further dried in vacuum at 70°C for 24 h.

To prepare the crystalline samples, neat S-iPP, neat S-sPP, and their blends were firstly annealed in the melt state (at 170°C) for 5 min to erase previous crystallization history followed by rapid cooling ($>100^\circ\text{C}/\text{min}$) to the desired T_c s for isothermal crystallizations for 3 h. Figure S1 shows the differential scanning calorimetry (DSC) isothermal scans of S-iPP/S-sPP 20/80 blend at different T_c s for 3 h to demonstrate that this time duration was sufficiently long to attain the saturated crystallinity, as evidenced by the fact that the isothermal crystallization exotherms were completely recorded in 20 min irrespective of T_c .

2.2 | Small angle X-ray scattering (SAXS) measurement

The morphology of the neat diblock copolymers and their blends was probed by SAXS at the Endstation BL23A1 of the National Synchrotron Radiation Research Center (NSRRC), Taiwan. The energy of the X-ray source and the sample-to-detector distance were 8 keV and 1815 mm, respectively. The scattering signals were collected by using

Pilatus-1MF detector of 981×1043 pixel resolution with a typical exposure time of 5 min. The scattering intensity profile was the output as the plot of the scattering intensity (I) versus the magnitude of the scattering vector, $q = (4\pi/\lambda) \sin(\theta/2)$ (θ = scattering angle). The SAXS profiles were corrected for the incident beam intensity, the detector sensitivity, and the background.

2.3 | Wide angle X-ray scattering (WAXS) measurement

The crystalline structure of iPP and sPP in the neat diblock copolymers and their blends was probed by WAXS conducted at the Wiggler Beamline 17A1 of the NSRRC, Taiwan. A triangular bent Si (111) single crystal was used to obtain a monochromatic beam of wavelength $\lambda = 1.54 \text{ \AA}$. The diffraction patterns were collected using imaging plates (Fuji BAS III, area = $20 \times 40 \text{ cm}^2$) having $100 \text{ }\mu\text{m}$ pixel resolution. In the present study, the WAXS profiles of the crystalline samples were measured as a function of temperature in a heating cycle. The sample was allowed to be equilibrated at each temperature for 5 min followed by data acquisition for 5 min.

2.4 | Differential scanning calorimetry (DSC) measurement

The melting behavior of iPP and sPP crystallites in the neat diblocks, and their blends was analyzed by a TA Instrument 2000 DSC equipped with the RCS cooling system. The DSC heating scans of the samples isothermally crystallized at the prescribed T_c s were recorded from 30 to 170°C at the heating rate of $5^\circ\text{C}/\text{min}$.

2.5 | Large-amplitude oscillatory shear (LAOS) experiment

The oriented sample of S-iPP/S-sPP 20/80 blend was prepared by using a Linkam CSS450 temperature-controlled shear system. The sample was reshaped into a thin disk of suitable thickness and diameter and held in the gap between the two glass windows. Subsequently, it was pressed by the two plates at 170°C and sheared for 1 h using the amplitude oscillatory mode via the bottom plate. The shear amplitude and the frequency applied were 80% and 0.2 Hz, respectively.

3 | RESULTS AND DISCUSSION

3.1 | Miscibility and morphology of S-iPP/S-sPP blends in the melt state

The SAXS profiles of S-iPP, S-sPP, and their blends collected at 170°C are shown in Figure 1A to study their melt morphology. Neat S-iPP displayed a broad scattering peak showing that the copolymer was in the disordered state due to weak segregation between iPP and PS blocks having low molecular weights. Neat S-sPP exhibited the double gyroid structure as revealed by a series of peaks with the position ratios of 1: $(4/3)^{1/2}$: $(7/3)^{1/2}$: $(10/3)^{1/2}$.⁴¹ However, the blends of these two diblock copolymers with the different composition ratios displayed the lamellar morphology, as evidenced by integral position ratios of the multiple scattering peaks. The formation of lamellar structure in the S-iPP/S-sPP blends signaled that the constituent blocks from the two copolymers were miscible in their respective microdomains, considering the compositions of PS component in the

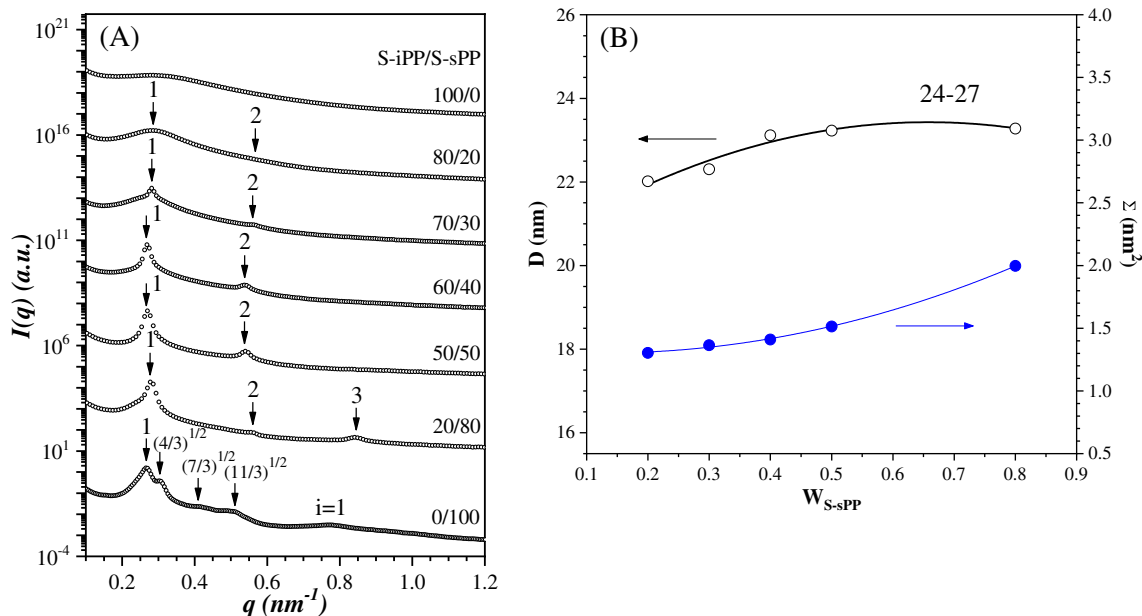


FIGURE 1 (A) SAXS profiles of S-iPP, S-sPP, and S-iPP/S-sPP blends collected in the melt state (at 170°C). (B) Variations of the interlamellar distance (D) and the area per junction point at the lamellar interface (Σ) as a function of the weight fraction of S-sPP in the blends

blends were nearly symmetric, with its overall volume fraction ranging from 0.46 to 0.52. This was in clear contrast to the immiscibility of iPP and sPP homopolymers found in their blends.^{24–27}

The interlamellar distance (D) and the area per junction point at the lamellar interface (Σ) determined from the SAXS results are plotted against the weight fraction of S-sPP in Figure 1B, where Σ was given by¹²

$$\Sigma = \frac{2\{[(1-n_{S-sPP})N_{S-IP,PS} + n_{S-sPP}N_{S-sPP,PS}]V_{PS} + (1-n_{S-sPP})N_{S-iPP,iPP} + n_{S-sPP}N_{S-sPP,iPP}\}V_{PP}}{d} \quad (1)$$

where n_i ($i = S-iPP$ or $S-sPP$) denotes the number fraction of the diblock copolymer in the blends, $N_{S-iPP,PS}$, $N_{S-sPP,PS}$, $N_{S-iPP,iPP}$, and $N_{S-sPP,iPP}$ are the degrees of polymerization of PS, iPP, or sPP blocks, and V_j ($j = PS, iPP, \text{ or } sPP$) is the volume of a j monomer unit ($V_{PS} = 0.164 \text{ nm}^3$, $V_{iPP} = 0.0815 \text{ nm}^3$, and $V_{sPP} = 0.0817 \text{ nm}^3$). As shown in Figure 1B, the interlamellar distance increased with increasing S-sPP content, as the PS and PP domains were swollen by the longer PS and sPP blocks from S-sPP, respectively. This further attests that the PS blocks and the iPP and sPP blocks from the two copolymers mixed in their respective microdomains. On the other hand, upon the addition of S-sPP, the cross sectional area of the junction point, Σ , was swollen instead of remaining constant predicted by the co-surfactant model.^{11,12} This was likely due to the fact that the blends were located near the weak segregation regime, such that the assumption of strong segregation with sharp interface underlying Equation (1) was not strictly valid.¹² Nevertheless, the phase behavior of the S-iPP/S-sPP blend system was basically in parallel with that found for the diblock blends exhibiting the co-surfactant effect.^{11,12} In other words, each lamellar domain was constituted of two layers of brushes lying on top of each other as schematically illustrated in Figure 2; the first layer adjacent to the microdomain interface was formed by the shorter blocks and the first subchains in the longer blocks, while the second layer located in the middle region of the microdomains was composed of the remaining subchains of the longer blocks.

3.2 | Crystallization behavior of iPP and sPP blocks within lamellar microdomains

Since the SAXS profiles of the samples were virtually unperturbed after the crystallization, the lamellar structure established in the melt state was effectively preserved over the T_c range investigated. That is, the crystallizations of iPP and sPP blocks were effectively confined within the lamellar microdomains. A DSC cooling experiment was performed to gain an initial insight into the crystallization behavior of iPP and sPP block in their common lamellar microdomains. Figure S2A displays the DSC cooling curves recorded in the cooling process. The crystallization exotherms associated with the crystallization of iPP block in the S-iPP/S-sPP blends were detectable at the temperatures close to that of neat S-iPP (see also Figure S2B showing the plot of the peak temperature of the exotherm, T_f , as a function of the weight

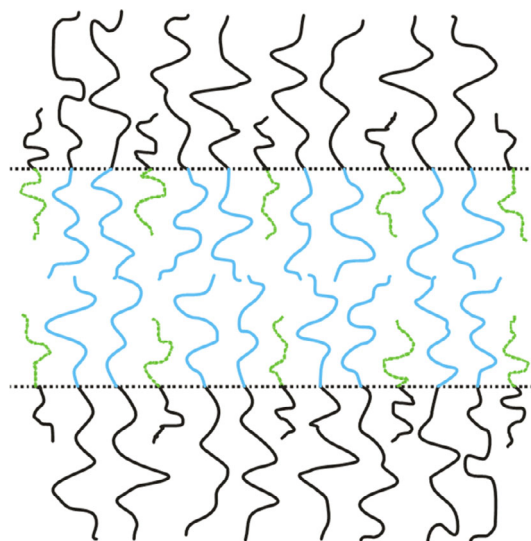


FIGURE 2 Schematic illustration of the co-surfactant model for the melt structure of the lamellae-forming S-iPP/S-sPP blends. The black, green, and blue lines represent PS, iPP, and sPP blocks, respectively

percentage of S-iPP in the blend), except for the 20/80 blend which exhibited a large shift of the iPP exotherm to lower temperature ($T_f \approx 85^\circ\text{C}$), leading to its significant overlap with the sPP exotherm. The two types of PP block in this blend thus showed comparable crystallization rates. On the other hand, the T_f of sPP block from S-sPP increased drastically upon blending with S-iPP due to the enhancement of its crystallization kinetics by the prior formed iPP crystallites that served as nucleation agent for the sPP crystallization. Nevertheless, once the S-iPP content was more than 70 wt%, the T_f of sPP block was not discernible probably because of the low level of crystallinity attainable with low sPP block composition. The co-crystallization of iPP and sPP blocks in the lamellar microdomains was precluded by the existence of two separated exotherms in the DSC cooling curves as well as the overlapped yet splitted melting endotherms obtained by the subsequent heating scans (see Figure S2C). The results of the non-isothermal DSC scans demonstrated that iPP and sPP blocks formed a miscible mixture in the PP domains, such that their respective crystallization kinetics was perturbed by the counterpart component when comparing to that associated with neat S-iPP and S-sPP.

Figure 3 displays the temperature-dependent WAXS profiles of S-iPP/S-sPP blends obtained by stepwise heating the samples having been isothermally crystallized at 30°C (the corresponding results of neat S-iPP and S-sPP can be found in Figure S3). α -form crystal of iPP exhibited six strong reflections at $2\theta = 14.13^\circ, 16.78^\circ, 18.33^\circ, 20.89^\circ, 21.34^\circ, \text{ and } 25.15^\circ$, corresponding to (110), (040), (130), [(111), (131), or complex], [(140), (041), or complex], and (060) diffraction planes, respectively.^{42,43} (117) reflection can also be found for iPP at $2\theta = 19.71^\circ$ once the γ -form crystal developed.^{42–44} Form I crystal of sPP was found to exhibit three reflections at $2\theta = 12.30^\circ, 15.97^\circ, \text{ and } 20.61^\circ$, corresponding to (200), [(010) or (020)], and (220)/(121)

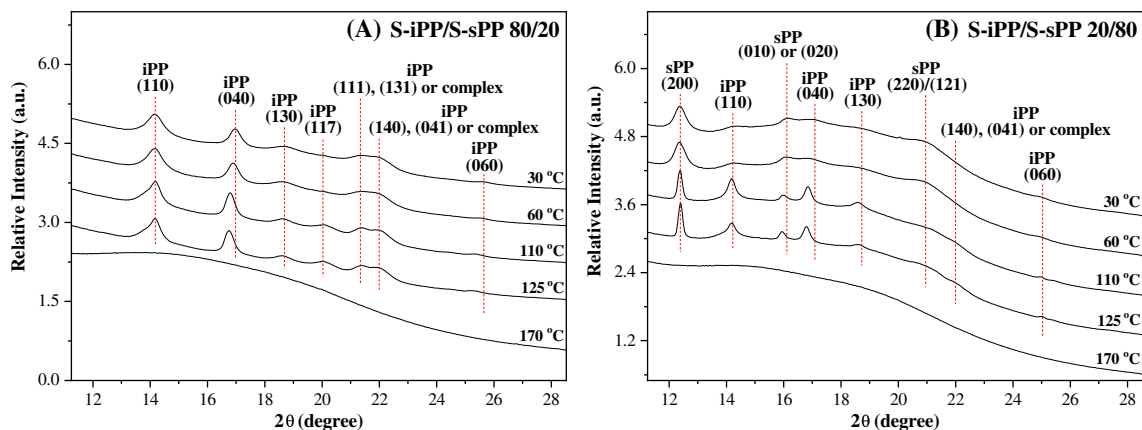


FIGURE 3 Temperature-dependent WAXS profiles of (a) S-iPP/S-sPP 80/20 and (b) S-iPP/S-sPP 20/80 blends collected after the samples have been isothermally annealed at 30°C for 3 h. For 20/80 blend, the broad peaks at $2\theta = 12.38^\circ$, 14.20° , 16.10° , 17.08° , 18.70° , 20.95° , 21.99° , and 25.03° were observed at the as-crystallized state, which however vanished and were replaced by the corresponding sharp diffraction peaks of iPP and sPP crystals upon heating to 110°C due to the significant occurrence of crystallization

diffractions, respectively.^{45–47} It can be seen in Figure 3 and Figure S3 that the characteristic diffraction peaks associated with iPP and sPP crystals were basically observable, demonstrating that iPP and sPP crystallites formed in the lamellar microdomains had identical crystallographic structures as those of the corresponding homopolymers. It is interesting to observe that the (117) and [(111), (131), or complex] peaks of the iPP blocks in both neat S-iPP (see Figure S3A) and the S-iPP/S-sPP 80/20 blend (see Figure 3A) emerged upon heating to 110°C, which was close to the glass transition temperature of PS block (T_g^{PS}). This indicates that the covalent connectivity with the vitrified PS block greatly impeded the chain mobility of iPP block for the formal crystallization, but once the temperature was raised above T_g^{PS} , the enhancement of chain mobility associated with the cold crystallization induced further development of both α - and γ -form crystals.

Close examination of the temperature-dependent WAXS profiles of the crystalline S-iPP-rich 80/20 blend in Figure 3A revealed that the crystallization at 30°C for the preparation of the as-crystallized sample was able to induce iPP crystallization, while under this crystallization protocol the crystallinity of sPP was essentially negligible. The iPP crystallinity thus attained was however lower in comparison to the corresponding homopolymer blend due to the constraint of the chemical junction with the vitrified PS blocks, which greatly limited the distance over which the iPP chains could be transported to the crystal growth front and the sPP blocks to be expelled away from the growth front during iPP crystallization. This type of crystal growth of iPP block was said to be “poisoned” by the surrounding sPP blocks.⁴⁸ Such a poisoning effect was severer for the crystallization of sPP block in this S-iPP-rich blend at 30°C, leading to nearly complete prohibition of its crystallization. Despite the enhancement of chain mobility allowed sPP to crystallize under the prescribed heating protocol to 110°C, the level of crystallinity attained was still very low, as demonstrated in Figure 3A.

The as-crystallized state of the S-sPP-rich 20/80 blend was found to display a series of broad peaks at $2\theta = 14.20^\circ$, 17.08° , 18.70° , 21.99° , and 25.03° and at $2\theta = 12.38^\circ$, 16.10° , and 20.95° associated

with iPP and sPP, respectively, in the WAXS profile (see Figure 3B). The large breadths and weak intensities of the diffraction peaks of iPP attested that the iPP crystallites formed in the lamellar microdomain at 30°C were very small. The diffraction peaks grew and sharpened significantly upon heating to 110°C; in particular, the peaks of α -form iPP crystals now became clear, showing that further crystallization of iPP blocks could take place within the time scale associated with the WAXS heating experiment due to enhancement of chain mobility.

To examine the thermodynamic stability of the crystalline structure formed in the S-sPP-rich blend, a DSC experiment was conducted to record the DSC heating scans of S-iPP/S-sPP 20/80 blend having been crystallized at different T_c s for 3 h, as shown in Figure 4. It is noted that the samples having been crystallized at the prescribed T_c s were rapidly cooled to 30°C (at $>100^\circ\text{C}/\text{min}$) followed by the DSC heating scans at $5^\circ\text{C}/\text{min}$. It can be seen that the samples crystallized at $T_c \leq 70^\circ\text{C}$ displayed a small endotherm (marked by T_m^1) before reaching T_m^{sPP} and T_m^{iPP} . For these T_c s, T_m^1 was found to locate at ca. 10°C higher than the corresponding T_c , and it was attributed to the melting of the small defective crystallites developed in the microdomain at $T_c \leq 70^\circ\text{C}$. These defective crystallites, which were not identified in the corresponding blends of iPP and sPP homopolymers (see Figure S4), gave rise to the broad peaks in the corresponding WAXS profiles observed at 30°C in Figure 3B. Considering that the crystallinities of sPP and iPP were low in this blend as-crystallized at 30°C (see the WAXS profile at 30°C in Figure 3B), the large melting endotherm observed at ca. 120°C was attributed to the melting of the crystals developed in the DSC heating process.

The WAXS and DSC results have revealed that, under the prescribed isothermal crystallization conditions at the different T_c s for 3 h, a population of highly defective crystallites with low melting point developed at sufficiently low T_c (i.e., $T_c \leq \sim 70^\circ\text{C}$) in S-sPP-rich blend. As further evidenced by the DSC results in Figure 4, these defective crystallites sustained up to ca. 10°C above the corresponding T_c . Here, it is postulated that the formation of the highly defective crystallites at low T_c was related to the highly restricted chain mobility of iPP and

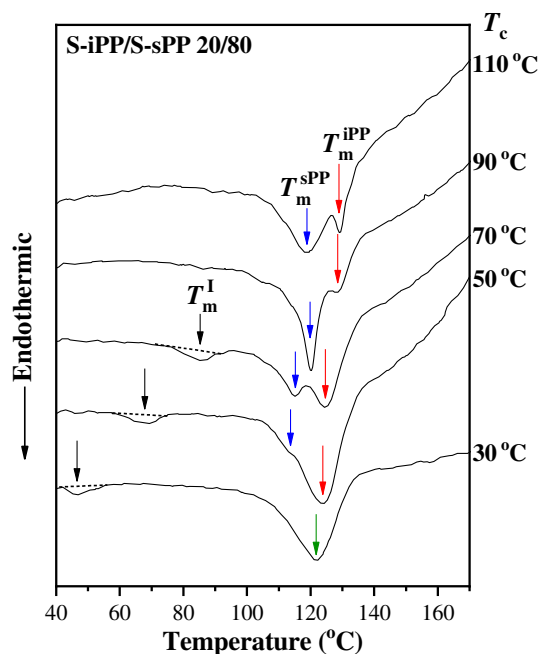


FIGURE 4 DSC heating scans of S-iPP/S-sPP 20/80 blend after isothermal crystallization at various T_c s for 3 h

sPP blocks in the PP microdomains. The similar hindrance to crystallization due to restricted chain mobility has also been observed in our previous study of a PS-*b*-PLLA/PS-*b*-PEO blend.¹⁴ To support this postulate, we calculated the mobility term associated with the crystallization kinetics defined as $M \sim \exp[-U^*/R(T_c - T_0)]$, with $U^* = 1500$ cal/mol and $T_0 = T_g^{PP} - 30$ being the activation energy associated with the transport of chain segments to the crystal growth front and the temperature at which such a transport ceases, respectively.^{49–51} Figure 5 displays the temperature variation of the mobility term; it can be seen that its magnitude increased abruptly at $T_c \cong 90^\circ\text{C}$, which was consistent with our postulate that the chain mobility associated with the crystallization of iPP and sPP blocks in the lamellar microdomain was highly restricted below 90°C , but it could be effectively released above this temperature.

On the basis of the above discussions, the development of the crystalline structure in S-sPP-rich blends is schematically illustrated in Figure 6. At sufficiently high T_c ($\geq 90^\circ\text{C}$), the higher chain mobility of both iPP and sPP blocks could induce the formal crystallization even under the influence of junction point constraint at the vitrified PS domain interface; as a result, the relatively high crystallinities were attained for both the iPP and sPP blocks, as illustrated in Figure 6A. The iPP and sPP crystallites thus formed exhibited a melting point at ca. 129 and 120°C , respectively. It is noted that amorphous iPP blocks were segregated locally due to the junction point constraint during the sPP crystallization, generating the amorphous regions surrounding the sPP crystallites in which the concentration of iPP was higher than the initial concentration for the subsequent iPP crystallization.

As for low T_c ($\leq 70^\circ\text{C}$), the strong junction point constraint and the highly restricted chain mobility of sPP blocks strongly hampered their formal crystallization. Nevertheless, a local demixing between a

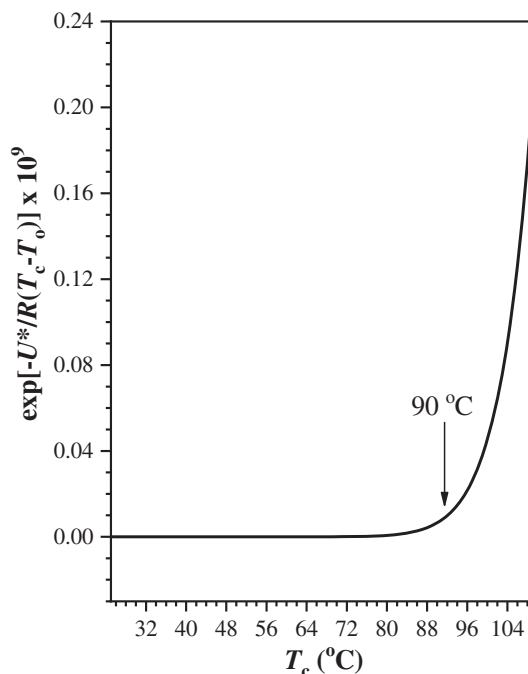
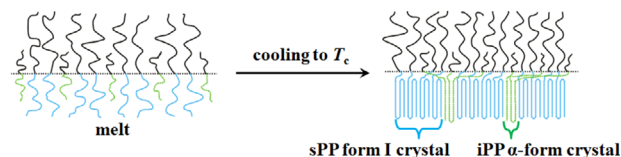


FIGURE 5 Dependence of the chain mobility term associated with the crystallization kinetics on T_c . The mobility term is defined as $M \sim \exp[-U^*/R(T_c - T_0)]$, where U^* ($= 1500$ cal/mol) is the activation energy associated with the transport of chain segments to the crystal growth front and T_0 ($= T_g - 30$, with $T_g^{PP} = -3^\circ\text{C}$ for S-iPP/S-sPP 20/80 blend) is the temperature at which such a transport ceases

(A) $T_c \geq 90^\circ\text{C}$



(B) $T_c \leq 70^\circ\text{C}$

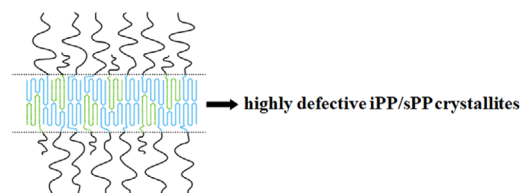
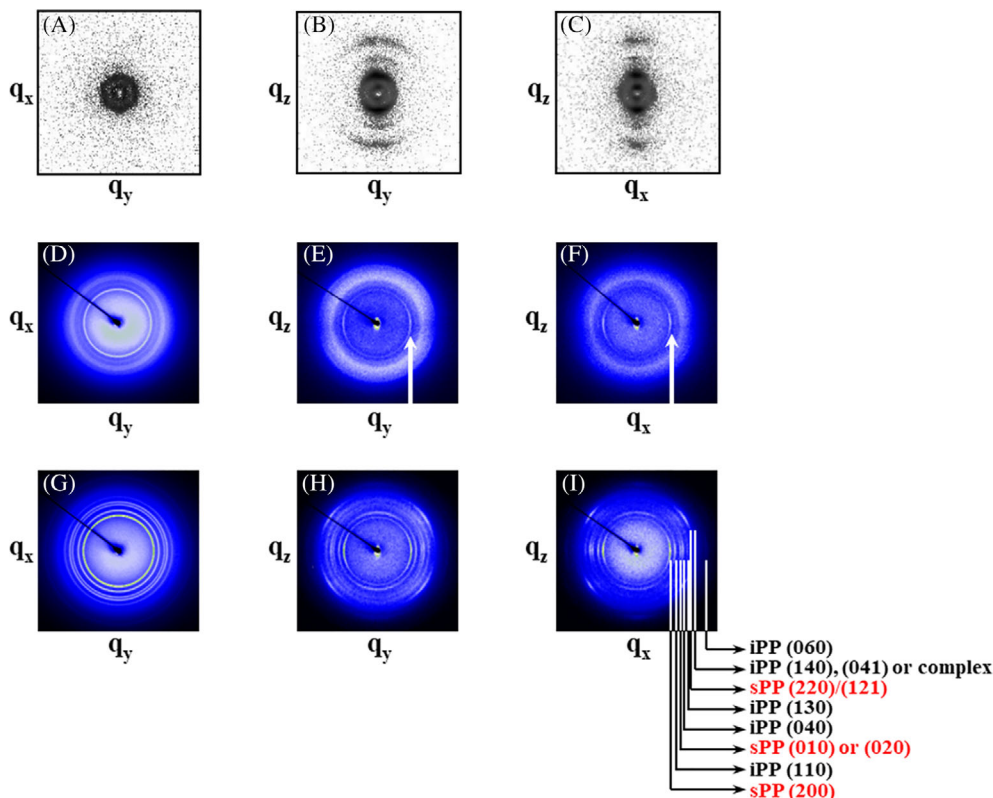


FIGURE 6 Schematic illustration of the crystalline structure development in S-sPP-rich blends. (A) At sufficiently high T_c ($\geq 90^\circ\text{C}$), the formal crystallization of iPP and sPP block chains could take place easily, thereby leading to relatively high iPP and sPP crystallinities. (B) At low T_c ($\leq 70^\circ\text{C}$), although the formal crystallization was strongly hampered, a local demixing between iPP and sPP chains might still take place and the demixed iPP and sPP chains organized to form the highly defective crystalline domains in which the iPP and sPP crystallites intervened each other

fraction of iPP and sPP block chains could still take place and the demixed iPP and sPP chains organized to form the defective crystalline domains in which the localized iPP and sPP crystallites intervened

FIGURE 7 (A–C) 2-D SAXS patterns collected along the tangential, radial, and normal directions (designated as x, y, and z, respectively) of the oriented S-iPP/S-sPP 20/80 blend. (D–F) 2-D WAXS patterns viewed along z, x, and y directions of 20/80 blend having been crystallized at 30°C. The arrows labeled in the patterns indicate that the defective crystalline domains exhibited a pair of arcs in the equator in the tangential and radial views. (G–I) 2-D WAXS patterns of 20/80 blend having been crystallized at 110°C, clearly exhibiting five iPP diffractions and three sPP diffractions. It was found that the crystalline stems of both iPP and sPP aligned normal to the lamellar interface as indicated by the feature of the 2-D patterns



each other, as schematically illustrated in Figure 6B. The defective iPP/sPP crystallites gave rise to broad peaks in the WAXS profiles and very low melting points located at only ca. 10°C higher than the corresponding T_c s due to the contribution of an excess surface free energy at the interface between alternately intervened iPP and sPP crystallites.

3.3 | Preferred orientation of iPP/sPP crystallites in the lamellar microdomains

In this study, the crystal orientation of iPP and sPP within the 1-D lamellar microdomains of S-iPP/S-sPP 20/80 blend has also been examined. The oriented crystalline sample was prepared by LAOS in the melt state and followed by crystallization at the desired T_c upon the rapid quenching process as described in the experimental section. Figure 7A–C shows the 2-D SAXS patterns of the oriented blend sample viewed along the normal, tangential, and radial directions, designated as z, x, and y, respectively. The appearance of arcs in the 2-D SAXS patterns indicated that the blend sample with large-scale oriented microdomains was successfully prepared. The SAXS patterns further indicated that the lamellar microdomains stacked along the z direction, as evidenced by the almost identical 2-D patterns along x and y directions and the diffraction arcs locating at the meridians. However, the lamellar microdomains adopted random orientation when viewed along the layer normal direction, as suggested by the observation of only a weak isotropic ring in the 2-D pattern along the z direction.

The corresponding 2-D WAXS patterns along z, x, and y directions of the blend having been crystallized at 30°C is displayed in Figure 7D–F, respectively. The WAXS result in Figure 3B has shown that the crystalline phase in this sample predominately composed of the defective crystalline domains. It is interesting that these domains could still exhibit the anisotropic scattering patterns showing a pair of sharp arcs in the equator along tangential view and a pair of broad arcs in the meridians along radial view, while only an isotropic pattern in the normal view. Consequently, the defective crystallites displayed the highly preferred orientation when viewed along x and y directions (but the orientation with looking through the z direction was rather random). Once the formal crystallization of iPP and sPP blocks occurred at the higher T_c (e.g., 110°C), the strong diffractions of iPP and sPP crystals were discernible in the 2-D WAXS patterns as displayed in Figure 7G–I. Particularly, the (040) arcs of iPP and (010) or (020) arcs of sPP appeared clearly at the equator in the tangential and radial views, revealing that the crystalline stems of both iPP and sPP aligned normal to the lamellar interface.

4 | CONCLUSIONS

We have studied the morphology and crystallization behavior in the binary blends of S-iPP and S-sPP diblock copolymers. The PS blocks from the two copolymers mixed intimately in the PS lamellar microdomains in the melt state; furthermore, iPP and sPP blocks were found to also form a miscible mixture in their common lamellar microdomains. Thus, iPP and sPP, which were immiscible in their

homopolymer blend, could become miscible in the microdomains formed by their diblock copolymer blend, in that the gain of conformational entropy and entropy of mixing may compensate the increase of interaction energy. The lamellar structure formed in the melt state was preserved after crystallizations of iPP and sPP blocks, indicating that the crystallization was effectively confined in the PP microdomain. Under the influences of the intimate mixing and the junction point constraint, the crystallization behavior of both iPP and sPP blocks in S-sPP-rich blends was significantly perturbed in comparison to that in the neat diblock copolymers. At sufficiently low T_c ($\leq 70^\circ\text{C}$), the restricted chain mobility and junction point constraint strongly hampered the formal crystallizations of the α -form iPP crystals and the form I sPP crystals; nevertheless, a local demixing between a fraction of iPP and sPP block chains could still take place and the demixed iPP and sPP chains organized to form the highly defective crystalline domains, in which the iPP and sPP crystals intervened each other. These domains exhibited a low melting point located at around 10°C higher than the corresponding T_c and gave rise to the broad peaks in the WAXS profiles. Finally, the crystal orientation in the macroscopically oriented S-iPP/S-sPP 20/80 blend having been crystallized at $T_c = 110^\circ\text{C}$ was also studied, revealing that both the iPP and sPP crystalline stems formed within the lamellar microdomains oriented normal to the lamellar interface.

ACKNOWLEDGMENTS

This work is supported by the Ministry of Science and Technology (MOST), Taiwan under Grant No. MOST 108-2221-E-007-021. The authors appreciate the beamtime of BL23A1 and BL17A1 provided by NSRRC in Taiwan.

ORCID

Che-Yi Chu  <https://orcid.org/0000-0002-8482-903X>

Hsin-Lung Chen  <https://orcid.org/0000-0002-3572-723X>

REFERENCES

- [1] L. Zhu, S. Z. D. Cheng, B. H. Calhoun, Q. Ge, R. P. Quirk, E. L. Thomas, B. S. Hsiao, F. Yeh, B. Lotz, *J. Am. Chem. Soc.* **2000**, *122*, 5957.
- [2] Y. L. Loo, R. A. Register, in *Developments in Block Copolymer Science and Technology* (Ed: I. W. Hamely), John Wiley & Sons, Ltd, New York **2004** Chapter 6.
- [3] G. Reiter, G. Castelein, J. U. Sommer, in *Polymer Crystallization: Observations, Concepts and Interpretations* (Eds: G. Reiter, J. U. Sommer), Springer, Berlin **2003** Chapter 8.
- [4] A. J. Müller, V. Balsamo, M. L. Arnal, T. Jakob, H. Schmalz, V. Abetz, *Macromolecules* **2002**, *35*, 3048.
- [5] A. J. Müller, V. Balsamo, M. L. Arnal, *Adv. Polym. Sci.* **2005**, *190*, 1.
- [6] L. Sangroniz, D. Cavallo, A. J. Müller, *Macromolecules* **2020**, *53*, 4581.
- [7] N. L. Meereboer, I. Terzic, S. Saidi, D. H. Merino, K. Loos, *ACS Macro Lett.* **2018**, *7*, 863.
- [8] P. Huang, L. Zhu, S. Z. D. Cheng, Q. Ge, R. P. Quirk, E. L. Thomas, B. Lotz, B. S. Hsiao, L. Liu, F. Yeh, *Macromolecules* **2001**, *34*, 6649.
- [9] M. S. Hsiao, J. X. Zheng, S. W. Leng, R. M. Van Horn, R. P. Quirk, E. L. Thomas, H. L. Chen, B. S. Hsiao, L. Rong, B. Lotz, S. Z. D. Cheng, *Macromolecules* **2008**, *41*, 8114.
- [10] M. C. Lin, Y. C. Wang, H. L. Chen, A. J. Müller, C. J. Su, U. S. Jeng, *J. Phys. Chem. B* **2011**, *115*, 2494.
- [11] F. Court, T. Hashimoto, *Macromolecules* **2001**, *34*, 2536.
- [12] F. Court, T. Hashimoto, *Macromolecules* **2002**, *35*, 2566.
- [13] Y. Y. Huang, B. Nandan, H. L. Chen, C. S. Liao, U. S. Jeng, *Macromolecules* **2004**, *37*, 8175.
- [14] C. Y. Chu, H. L. Chen, M. S. Hsiao, J. H. Chen, B. Nandan, *Macromolecules* **2010**, *43*, 3376.
- [15] H. Younes, D. Cohn, *Eur. Polym. J.* **1988**, *24*, 765.
- [16] C. Nakafuku, M. Sakoda, *Polym. J.* **1993**, *25*, 909.
- [17] C. Nakafuku, *Polym. J.* **1996**, *28*, 568.
- [18] A. J. Nijenhuis, E. Colstee, D. W. Grijpma, A. J. Pennings, *Polymer* **1996**, *37*, 5849.
- [19] J. M. Yang, H. L. Chen, J. W. You, J. C. Hwang, *Polym. J.* **1997**, *29*, 657.
- [20] H. Mao, M. A. Hillmyer, *Macromol. Chem. Phys.* **2008**, *209*, 1647.
- [21] H. Mao, P. L. Arrechea, T. S. Bailey, B. J. S. Johnson, M. A. Hillmyer, *Faraday Discuss.* **2005**, *128*, 149.
- [22] H. Mao, M. A. Hillmyer, *Soft Matter* **2006**, *2*, 57.
- [23] Y. W. Chen, B. J. Yeh, T. Hashimoto, S. Y. Liao, C. T. Lo, *Macromolecules* **2018**, *51*, 7699.
- [24] R. Thomann, J. Kressler, S. Setz, C. Wang, R. Mülhaupt, *Polymer* **1996**, *37*, 2627.
- [25] R. Thomann, J. Kressler, B. Rudolf, R. Mülhaupt, *Polymer* **1996**, *37*, 2635.
- [26] R. D. Maier, R. Thomann, J. Kressler, R. Mülhaupt, B. Rudolf, *J. Polym. Sci., Part B* **1997**, *35*, 1135.
- [27] T. C. Clancy, M. Pütz, J. D. Weinhold, J. G. Curro, W. L. Mattice, *Macromolecules* **2000**, *33*, 9452.
- [28] G. Natta, P. Corradini, *Il Nuovo Cimento* **1960**, *15*, 40.
- [29] S. V. Meille, D. R. Ferro, S. Brückner, A. J. Lovinger, F. J. Padden, *Macromolecules* **1994**, *27*, 2615.
- [30] D. R. Morrow, B. A. Newman, *J. Appl. Phys.* **1968**, *39*, 4944.
- [31] S. V. Meille, S. Brückner, W. Porzio, *Macromolecules* **1990**, *23*, 4114.
- [32] T. Konishi, K. Nishida, T. Kanaya, *Macromolecules* **2006**, *39*, 8035.
- [33] B. Lotz, A. J. Lovinger, R. E. Cais, *Macromolecules* **1988**, *21*, 2375.
- [34] A. J. Lovinger, B. Lotz, D. D. Davis, *Polymer* **1990**, *31*, 2253.
- [35] C. D. Rosa, F. Auriemma, V. Vinti, *Macromolecules* **1998**, *31*, 7430.
- [36] C. D. Rosa, P. Corradini, *Macromolecules* **1993**, *26*, 5711.
- [37] F. Auriemma, C. D. Rosa, O. R. D. Ballesteros, V. Vinti, P. Corradini, *J. Polym. Sci., Part B: Polym. Phys.* **1998**, *36*, 395.
- [38] V. Vittoria, L. Guadagno, A. Comotti, R. Simonutti, F. Auriemma, C. D. Rosa, *Macromolecules* **2000**, *33*, 6200.
- [39] J. C. Tsai, J. C. Kuo, R. M. Ho, T. M. Chung, *Macromolecules* **2006**, *39*, 7520.
- [40] M. C. Lin, H. L. Chen, W. F. Lin, P. S. Huang, J. C. Tsai, *J. Phys. Chem. B* **2012**, *116*, 12357.
- [41] C. Y. Chu, W. F. Lin, J. C. Tsai, C. S. Lai, S. C. Lo, H. L. Chen, T. Hashimoto, *Macromolecules* **2012**, *45*, 2471.
- [42] S. V. Meille, P. J. Phillips, K. Mezghani, S. Brückner, *Macromolecules* **1996**, *29*, 795.
- [43] Q. Gou, H. Li, Z. Yu, E. Chen, Y. Zhang, S. Yan, *Colloid Polym. Sci.* **2007**, *285*, 1149.
- [44] S. V. Meille, S. Brückner, *Nature* **1989**, *340*, 455.
- [45] N. Naga, K. Mizunuma, H. Sadatoshi, M. Kakugo, *Polymer* **2000**, *41*, 203.
- [46] M. Grasruck, G. Strobl, *Macromolecules* **2003**, *36*, 86.
- [47] C. D. Rosa, F. Auriemma, *Prog. Polym. Sci.* **2006**, *31*, 145.
- [48] G. Ungar, E. G. R. Putra, D. S. M. de Silva, M. A. Scherbina, A. J. Waddon, *Adv. Polym. Sci.* **2005**, *180*, 45.
- [49] J. I. Lauritzen Jr., J. D. Hoffman, *J. App. Phys.* **1973**, *44*, 4340.
- [50] S. Z. D. Cheng, J. J. Janimak, A. Zhang, H. N. Cheng, *Macromolecules* **1990**, *23*, 298.

- [51] J. Rodriguez-Arnold, Z. Bu, S. Z. D. Cheng, E. T. Hsieh, T. W. Johnson, R. G. Geerts, S. J. Palackal, G. R. Hawley, M. B. Welch, *Polymer* **1994**, 35, 5194.

SUPPORTING INFORMATION

Additional supporting information may be found in the online version of the article at the publisher's website.

How to cite this article: C.-Y. Chu, M.-Z. Chen, W.-H. Li, J.-C. Tsai, H.-L. Chen, *Polym. Cryst.* **2021**, 4(6), e10213. <https://doi.org/10.1002/pcr2.10213>